Mechanics of Materials 209 (2025) 105409

Contents lists available at ScienceDirect

Mechanics of Materials

journal homepage: www.elsevier.com/locate/mecmat

Research paper

Thermo-mechanical behavior of three-phase shape memory polymers for a wide temperature change

Suyeong Jin [a], Gunho Kim [b], Seola Lee [b], Kamakshi Subramanian [c], Jung-Wuk Hong [a,*], Chiara Daraio [b,*]

[a] Department of Civil and Environmental Engineering, Korea Advanced Institute of Science and Technology, 291 Deahak-ro, Yuseong-gu, Daejeon 34141, Republic of Korea
[b] Division of Engineering and Applied Science, California Institute of Technology, Pasadena, CA 91125, USA
[c] Department of Physics and Astronomy, Wellesley College, Wellesley, MA 02481, USA

ARTICLE INFO

Keywords:
Shape memory polymers (SMPs)
Thermo-mechanical testing
Three-phase model
Phenomenological model
Crystallization

ABSTRACT

Shape memory polymers (SMPs) are advanced materials capable of recovering their original configuration in response to external stimuli such as heat, light, and electric or magnetic fields. These properties demonstrate their potential in applications like deployable morphing structures in aerospace, vessel embolization, and flexible tools for minimally invasive surgical procedures in medicine. SMPs exhibit complex behaviors, including shape recovery, stress relaxation, and phase transitions (e.g., from rubbery to glassy states), which are challenging to capture through experimental methods alone. Numerical models provide an effective means to analyze these behaviors under various multiphysics conditions, facilitating the systematic exploration of material properties to optimize performance across applications. However, existing models typically focus on behavior before the crystalline phase, leaving a gap in understanding its performance in the crystalline phase, where thermo-mechanical properties may change at temperatures lower than those in the glassy state. In this study, we investigate SMP response over a broad temperature range and propose a new phenomenological three-phase model that accounts for interactions among the rubbery, glassy, and crystalline phases under one-dimensional uniaxial loading conditions. Isothermal tests examine the stress-strain behavior at fixed temperatures, while thermo-mechanical tests are used to investigate phase transitions. The numerical model, developed from experimental data, demonstrates the potential to accurately predict SMP behavior across a wide temperature range. This study lays the groundwork for applying the proposed model to multi-phase systems, enabling the prediction of SMP behavior under varying thermo-mechanical conditions.

1. Introduction

Shape memory polymers (SMPs) are smart materials that revert to a permanent configuration from a previously fixed temporary shape upon exposure to an external stimulus (Ge et al., 2016). SMPs are capable of undergoing large deformations and exhibit tunable mechanical properties, which are influenced by the methods used during synthesis. Specifically, the transition temperature can be controlled by adjusting the degree of crosslinking (Xiao et al., 2015; Liu et al., 2002; Risso et al., 2024). Various external stimuli, including heat, electricity, light, magnetism, moisture, and changes in pH, can induce macroscopic deformation in SMPs (Leng et al., 2011). Depending on their intended function, SMPs can be manufactured as one-way, two-way, or multi-way systems (Wang et al., 2019; Zeng et al., 2021).

Due to their ability to respond to external stimuli, SMPs hold significant potential across a wide range of applications, including biomedical devices, soft robotics, aerospace engineering, shape memory arrays, and 4D printing (Xia et al., 2021; Shojaei et al., 2022). For example, SMP sutures were prototyped for wound closure in response to thermal stimuli (Lendlein and Langer, 2002), and SMP-based embolization devices were developed for the treatment of saccular aneurysms (Boyle et al., 2016). In aerospace engineering, SMP composites were explored for deployable and morphing structures (Wei et al., 2015; Al Azzawi et al., 2019).

Various numerical models for SMPs have been developed to accurately predict their behavior under diverse conditions, as the scope of SMP application continues to expand (Yan and Li, 2022). A modified standard linear viscoelastic model has been proposed, with temperature -dependent coefficients for the model elements (Tobushi et al., 2001). A viscoelastic rheological model was constructed using the Prony series

* Corresponding author.
E-mail addresses: j.hong@kaist.ac.kr, jwhong@alum.mit.edu, jungwukh@gmail.com (J.-W. Hong), daraio@caltech.edu (C. Daraio).

https://doi.org/10.1016/j.mechmat.2025.105409
Received 26 March 2025; Received in revised form 2 June 2025; Accepted 2 June 2025
Available online 9 July 2025

and the time–temperature superposition principle to predict the self-folding behavior of SMPs (Mailen et al., 2015). A phase transition framework was employed to develop a viscoelastic SMP model consisting of active and frozen phases, with the volume fraction of these phases being temperature-dependent (Liu et al., 2006). A viscoelastic hard segment was serially connected to the hyperelastic soft segments of active and frozen phases to model shape memory polyurethanes (Kim et al., 2010). Additionally, multiplicative decomposition of the deformation gradient was incorporated into the glassy and rubbery phase framework to develop a three-dimensional SMP model (Park et al., 2016). In this model, the glassy phase includes viscoelastic, viscoplastic, and shape memory strain components, while the rubbery phase consists solely of viscoelastic components.

Numerical models for SMPs have been developed for the temperature range prior to the onset of the crystalline phase. The phase transition framework primarily focuses on the responses of the glassy and rubbery phases, without accounting for the crystalline state. While a temperature-dependent modulus of elasticity in the glass transition region was defined, the modulus was treated as a constant below this region (Tobushi et al., 2001). In fact, it has been demonstrated that the cooling process of an elongated SMP increases stress at temperatures below the crystallization onset (Posada-Murcia et al., 2022). The transitional state is not solely defined by temperature; rather, it represents an intermediate structure formed by polymer chains during the transition from the amorphous to the crystalline state. It is essential to account for the crystalline state in order to predict the behavior of SMP across a wide temperature range.

In this paper, we examine the response of SMPs over a wide temperature range, including the crystalline state, and propose a phenomenological three-phase model to describe SMP behavior across this range, extending below the onset temperature of the crystalline phase, under one-dimensional uniaxial loading conditions. The phase transition framework is briefly explained, and the crystalline phase is introduced to complete the three-phase model. Experiments, including SMP manufacturing setup, isothermal tests, and thermo-mechanical tests, are conducted. Numerical analyses are performed to develop the SMP numerical model.

2. Two-phase shape memory model

The phenomenological two-phase model was developed by Park et al. (2016) and is composed of rubbery and glassy phases, which provide a phenomenological description of shape memory polymer (SMP) behavior, as shown in the schematic diagram within the dashed blue box in Figs. 1(a) and (b). Each phase consists of several elements that describe the response at low and high temperatures, as shown in Fig. 1(b). Utilizing the iso-strain feature of the two-phase model, the total deformation gradient $\mathbf{F}$ can be multiplicatively decomposed into the elastic, viscoelastic, and other deformation gradients expressed as

$$\mathbf{F} = \mathbf{F}_r = \mathbf{F}_r^e \cdot \mathbf{F}_r^v \tag{1}$$

$$= \mathbf{F}_g = \mathbf{F}_g^e \cdot \mathbf{F}_g^v \cdot \mathbf{F}_g^p \cdot \mathbf{F}_g^s, \tag{2}$$

where the subscripts r and g denote the rubbery and glassy phases, respectively. The superscript e, v, p, and s represent the hyperelastic spring, the viscoelastic component comprising a spring and Newtonian fluid dashpot, the viscoplastic component, and the shape memory strain element, respectively. For example, $\mathbf{F}_r^e$ denotes the deformation gradient of the hyperelastic spring in the rubbery phase. Each phase in the SMP model has a volume fraction that varies as a function of temperature, with the sum of the fractions equal to unity, expressed as $\xi_r + \xi_g = 1$, where ξ_r and ξ_g represent the rubbery and glassy volume fractions, respectively. The volume fraction at a temperature T can be determined through a relaxation test (Park et al., 2016) expressed as

$$\xi_g = \frac{P - P\left(T_h\right)}{P\left(T_l\right) - P\left(T_h\right)}, \quad \xi_r = 1 - \xi_g, \tag{3}$$

where P represents the nominal stress, and a temperature T is within the range of $T_l \le T \le T_h$, where T_l and T_h represent the glassy and rubbery phase temperatures, respectively. Regression analysis is performed on the experimental data to derive the function for the volume fraction, written as (Park et al., 2016)

$$\xi_g = \begin{cases} 1 & 1 < \xi_g^0, \\ \xi_g^0 & 0 \le \xi_g^0 \le 1, \\ 0 & \xi_g^0 < 0, \end{cases} \text{where } \xi_g^0 = \frac{a}{1+\exp\left(b\left(T-T_{\mathrm{tr}}\right)\right)} - d, \tag{4}$$

where a, b, T_{tr}, and d are the coefficients for the volume fraction formulation. The stress of the SMP model is assumed to be the superposition of the stresses in each phase, weighted by their respective volume fraction, as expressed by $\boldsymbol{\sigma} = \xi_r(T)\,\boldsymbol{\sigma}_r + \xi_g(T)\,\boldsymbol{\sigma}_g$, where T denotes the temperature. By applying the assumptions of superposed stress and volume unity, the volume fraction of each phase can be expressed as a function of temperature, as detailed in the literature (Park et al., 2016).

The hyperelasticity part is modeled as a nearly incompressible Mooney–Rivlin material, with the first-order strain energy function W expressed as

$$W\left(\bar{I}, \overline{II}, J\right) = C_{10}\left(\bar{I} - 3\right) + C_{01}\left(\overline{II} - 3\right) + \frac{1}{2}k\left(J-1\right)^2, \tag{5}$$

where $\bar{I}$ and $\overline{II}$ are the first and second invariants of the tensor $\bar{\mathbf{C}} = \bar{\mathbf{F}}^T \cdot \bar{\mathbf{F}}$, respectively, and where $\bar{\mathbf{F}} = J^{-\frac{1}{3}}\mathbf{F}$ and $J = \det(\mathbf{F})$. The symbols C_{10} and C_{01} represent the material constants, and κ is the bulk modulus. The viscoplastic part is modeled using the Perzyna model written as

$$\dot{\mathbf{F}}_g^p = \frac{1}{\mu_g^p}\left\langle f \right\rangle \frac{\partial f}{\partial \boldsymbol{\sigma}_g}, \tag{6}$$

where μ_g^p is a viscosity coefficient, and f is a yield function defined as

$$f\left(\boldsymbol{\sigma}_g, \alpha^p(t)\right) = \sqrt{\boldsymbol{\sigma}_g^{\mathrm{dev}} : \boldsymbol{\sigma}_g^{\mathrm{dev}}} - \left\{\sigma^Y + E^p\left(\alpha^p(t)\right)^2\right\}, \tag{7}$$

where $\boldsymbol{\sigma}_g^{\mathrm{dev}}$, σ^Y, E^p, and α^p are the deviatoric stress, yield strength, hardening modulus, and equivalent viscoplastic strain of the glassy phase, respectively. By substituting Eqs. (1) to (7) into the Clausius–Duhem inequality (Holzapfel, 2002), the constitutive equations for each phase are derived (Park et al., 2016). In particular, the constitutive equations for the one-dimensional (1D) rubbery phase are written as

$$\lambda = \lambda_r = \lambda_r^e \lambda_r^v, \tag{8}$$

$$\mu_r\left\{2\left(\lambda_r^v\right)^3 + \frac{1}{\left(\lambda_r^v\right)^3}\right\}\frac{\mathrm{d}\lambda_r^v}{\mathrm{d}t} = \frac{1}{2}\left\{h\left(\lambda_r^e, C_{10,r}^e, C_{01,r}^e\right) - h\left(\lambda_r^v, C_{10,r}^v, C_{01,r}^v\right)\right\}, \tag{9}$$

$$h\left(\lambda, C_{10}, C_{01}\right) = 2C_{10}\left(\lambda^2 - \lambda^{-1}\right) + 2C_{01}\left(\lambda - \lambda^{-2}\right), \tag{10}$$

$$\sigma_r = h\left(\lambda, C_{10,r}^e, C_{01,r}^e\right), \tag{11}$$

where μ_r is the viscosity coefficient, λ is the stretch of the shape memory, C_{10} and C_{01} are the coefficients associated with the Mooney–Rivlin hyperelasticity, and σ_r is the Cauchy stress of the rubbery phase, determined by Mooney–Rivlin hyperelasticity.

The constitutive equations of the glassy phase are expressed as

$$\lambda = \lambda_g = \lambda_g^e \lambda_g^v \lambda_g^p \lambda_g^s, \tag{12}$$

$$\mu_g\left\{2\left(\lambda_g^v\right)^3 + \frac{1}{\left(\lambda_g^v\right)^3}\right\}\frac{\mathrm{d}\lambda_g^v}{\mathrm{d}t} = \frac{1}{2}\left\{h\left(\lambda_g^e, C_{10,g}^e, C_{01,g}^e\right) - h\left(\lambda_g^v, C_{10,g}^v, C_{01,g}^v\right)\right\}, \tag{13}$$

$$\dot{\lambda}_g^p = \frac{1}{\mu_g^p}\left\langle f \right\rangle \mathrm{sign}\left(\sigma_g\right), \tag{14}$$

$$f = \sigma_g - \left\{\sigma^Y + E^p\left(\alpha^p(t)\right)^2\right\},$$

$$\sigma_g = h\left(\lambda_g^e, C_{10,g}^e, C_{01,g}^e\right), \tag{15}$$

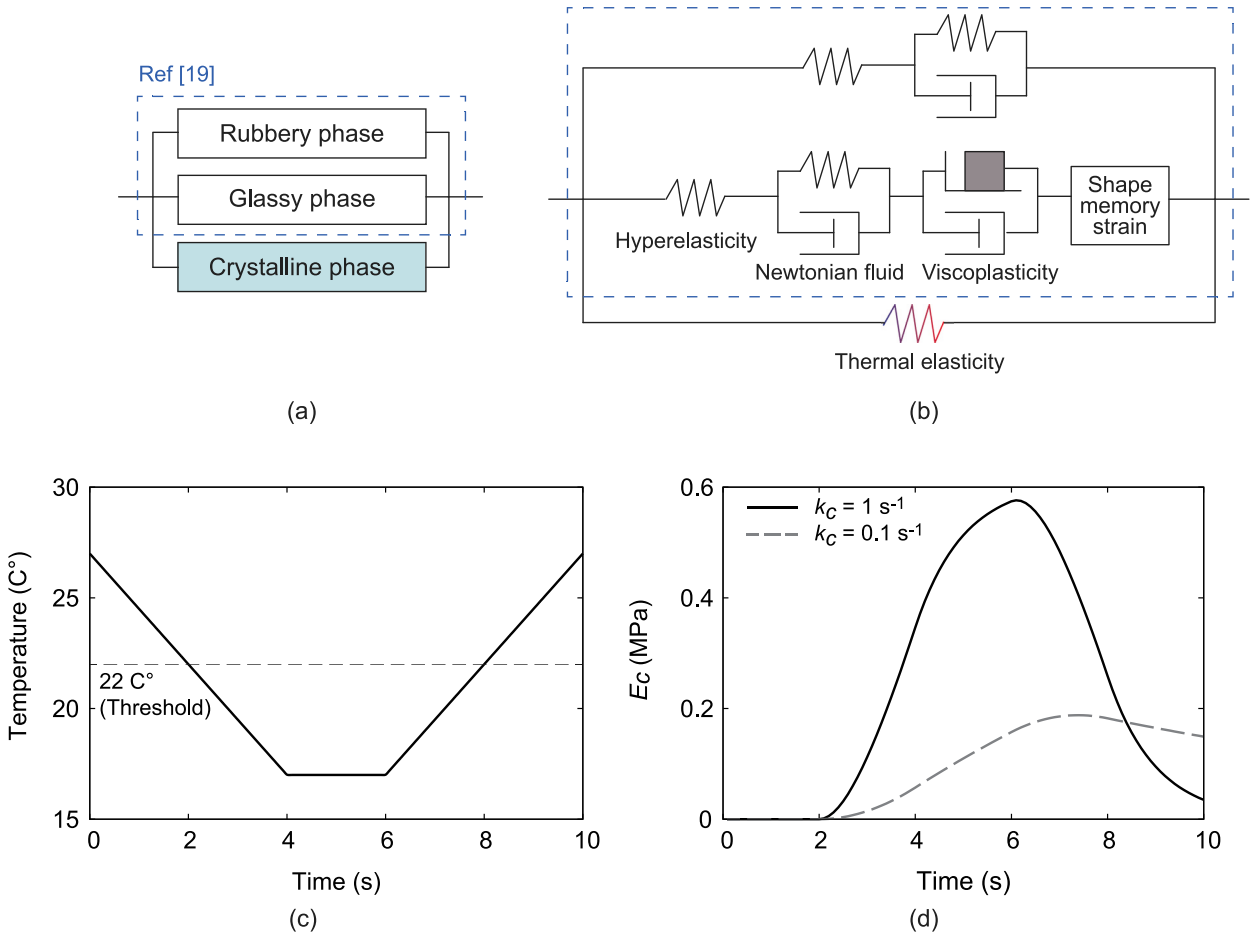

Fig. 1. Schematic of the proposed three-phase model: (a) Overview of the rubbery, glassy, and crystalline phases in parallel for the phenomenological description of SMP behavior; (b) Component elements of each phase. Specifically, in the crystalline phase, the thermal elasticity component is defined using the crystalline stiffness E_c, as expressed in Eqs. (19) and (20). An example of the time-varying E_c with temperature is shown: (c) Time-varying temperature conditions; and (d) Corresponding E_c.

$$\alpha^p(t) = \int_0^t \frac{\dot{\lambda}_g^p}{\lambda_g^p} \mathrm{d}t, \tag{16}$$

$$E_g^s = E_{g11}^s = \frac{\left(\lambda_g^s\right)^2 - 1}{2}, E_{g22}^s = E_{g33}^s = \frac{1}{2}\left(\frac{1}{\lambda_g^s} - 1\right), \tag{17}$$

$$\frac{\mathrm{d}E_g^s}{\mathrm{d}t} = \begin{cases} \alpha\xi_r\left(-E_g^s + \beta E\right) & \text{if } \beta\sum_{i=1}^3 \left(E_{ii}\right)^2 > \sum_{i=1}^3 \left(E_{ii}^s\right)^2, \\ \alpha\xi_r\left(-E_g^s + E\right) & \text{if } \beta\sum_{i=1}^3 \left(E_{ii}\right)^2 < \sum_{i=1}^3 \left(E_{ii}^s\right)^2, \end{cases} \tag{18}$$

where α and β are parameters associated with shape memory strains, and σ_g is the Cauchy stress of the glassy phase. Although the two-phase formulation is not intended to suggest thermodynamic coexistence of distinct phases, it is employed as a phenomenological approach to capture the gradual changes in mechanical properties during temperature variation (Chen and Lagoudas, 2008; Tobushi et al., 1997). The term *glassy phase* is used in a phenomenological sense to represent the regime exhibiting viscoplastic behavior and shape memory strain, and does not indicate a full transition to the glassy state defined by the glass transition temperature (T_g) (Risso et al., 2024).

Melting and crystallization temperatures are typically determined using differential scanning calorimetry (DSC), with each temperature corresponding to the peak amplitude in the thermal response. In the two-phase model, the melting temperature is commonly regarded as the onset temperature of the rubbery phase, while the crystallization temperature is considered the onset temperature of the glassy phase. The temperature range between these two values corresponds to a mixed phase of rubbery and glassy states. However, the two-phase model can only predict the deformation of SMPs within the temperature range before the crystalline phase. It is noted that crystallization can occur at room temperature; therefore, understanding the SMP crystalline behavior at this temperature is crucial for real-world applications.

3. Three-phase constitutive model

A three-phase SMP model is proposed in this section. The response of SMPs below the crystallization temperature has been examined in the literature (Posada-Murcia et al., 2022); cooling of stretched, chemically cross-linked polymers initiates the crystallization process, leading to a decrease in stress under constant strain conditions. Once the temperature drops below a certain threshold, the stress increases. The increase in stress observed at low temperatures under constant strain conditions is difficult to explain using the two-phase model.

A three-phase model is proposed to describe SMP behavior across a wide temperature range by introducing a crystalline phase, which is connected in parallel to the two-phase model, as shown in Fig. 1. The phases are modeled as connected in parallel, corresponding to the upper bound in composite theory, as a phenomenological approximation to capture the smooth transition in stiffness during the glass transition under uniaxial loading conditions (Chen and Lagoudas, 2008; Tobushi et al., 1997; Qi et al., 2008). The crystalline phase consists of a thermal elastic spring, which is activated when the temperature drops below

the crystallization threshold. The crystalline stiffness E_c of the spring is defined as a function of temperature T, growth rate k_c, the current amount of crystallization (considering the difference between E_c and saturated stiffness E_c^0), and the maximum saturation ratio γ, expressed as

$$\frac{\mathrm{d}E_c}{\mathrm{d}t} = k_c\left(-E_c + \gamma E_c^0\right), \tag{19}$$

$$E_c^0 = \begin{cases} \zeta\left(T - T_c\right) & \text{if } T < T_c, \\ 0 & \text{Otherwise,} \end{cases} \tag{20}$$

where T_c is the threshold temperature at which crystallization begins, and ζ is the coefficient with units of pressure per temperature. For example, we impose the temperature condition, as shown in Fig. 1(c), and set the crystallization temperature threshold to 22 °C. The crystalline phase begins at time $t = 2$ s. The crystalline stiffness E_c is calculated using Eqs. (19) and (20). Here, γ is set to unity, and ζ is set to −0.1222 MPa/°C. Then, Fig. 1(d) shows E_c as a function of temperature, increasing over time starting from $t = 2$ s, with different rates depending on k_c. This formulation is supported by experimental observations of stress evolution over time at constant temperature (Posada-Murcia et al., 2022; Callister Jr. and Rethwisch, 2020). The time-dependent behavior of the crystalline modulus serves as a phenomenological representation of the evolving microstructure, such as increasing crystallinity or reorganization, during isothermal crystallization, which leads to observable changes in the overall mechanical response.

The thermal elastic spring part is modeled using linear elasticity, and the constitutive equations for the crystalline phase are expressed as

$$\lambda = \lambda_c, \tag{21}$$

$$\sigma_c = E_c\left(\lambda_c - 1\right), \tag{22}$$

where λ_c and σ_c represent the stretch and Cauchy stress of the crystalline phase, respectively, and the total stress applied to the SMP is calculated as

$$\sigma = \xi_g\sigma_g + \xi_r\sigma_r + \sigma_c. \tag{23}$$

4. Experiments on shape memory polymers (SMPs)

4.1. Manufacturing of shape memory polymer

Polycyclooctene (PCO) and dibenzoyl peroxide (DBzP) were dissolved in toluene ($C_6H_5CH_3$) to form an opaque solution, using 2.5 wt% DBzP relative to PCO. The solution was initially dried using a rotary evaporator (rotavap) at 50 °C for 2 h, followed by vacuum drying on a Schlenk line for 48 h with a dry ice-acetone vapor trap. This process yielded a white polymer chunk with a homogeneous mixture of PCO and DBzP.

To fabricate dog-bone samples, the polymer chunks containing the crosslinker were sliced into thin pieces with a thickness of approximately 1 mm. These slices were compressed into a mold and crosslinked in a vacuum oven. For this step, a Teflon plate, with a thickness of 10 mm and an area of 170 × 75 mm^2, engraved with the mold, was fabricated using CNC machining. The polymer slices were placed into the mold and heated in an oven at 60 °C without vacuum. During this stage, the polymer melted and filled the mold, ensuring the absence of air bubbles.

Following the initial melting step, the mold was tightly sealed with a Teflon lid and secured using C-clamps. The temperature was then increased to 91 °C, and the sample was cured under vacuum for 72 h. Once the curing process was complete, the samples were cooled to room temperature and carefully removed from the molds. A visual inspection was conducted to check for air bubbles, ensuring that the mechanical properties of the dog-bone samples were not compromised.

4.2. Differential scanning calorimetry (DCS) analysis of the crystallization temperature

The melt transition (T_m) and crystallization (T_c) temperatures as a function of the crosslinker dibenzoyl peroxide (DBzP) loading were previously reported by Risso et al. (2024). These temperatures were determined using differential scanning calorimetry (DSC) analysis. For the PCO SMP with 2.5 wt% DBzP, the T_m and T_c were calculated from regression data to be 49.7 °C and 22.8 °C, respectively.

4.3. Isothermal test at a constant temperature

Firstly, an isothermal cyclic loading test was conducted at a high temperature of 65 °C to obtain the rubbery behavior of SMPs. The SMP specimen was fabricated using the Dumbbell-shaped ISO 37 Type 4 geometry, with a thickness of 1 mm, and was gripped at both ends in the dynamic mechanical analysis (DMA) machine, as shown in Fig. A.2. The specimen was initially stretched to a displacement of 7.93 mm at a loading rate of 85.34 mm/min, followed by a 1800 s hold for stress relaxation. Unloading was performed by releasing the stress at a rate of 15 N/min, and the recovery displacement was measured for 30 minutes. To ensure stable data collection, a preload of 10^{-4} N was applied and maintained during the recovery measurement.

As a result, Fig. 2(a) shows the graph of engineering strain versus time at a constant temperature of 65 °C. The strain increases rapidly until the maximum displacement is reached, then decreases due to stress relaxation until 2000 s. Upon unloading, the strain recovers to nearly its original value. Fig. 2(b) shows the graph of nominal stress versus time. The stress initially increases to 0.3 MPa, then decreases due to stress relaxation.

Secondly, an isothermal cyclic loading test was performed at a low temperature of 35 °C to obtain the glassy behavior of SMPs. The specimen geometry is the same as shown in Fig. A.2 with a thickness of 1 mm. The specimen was gripped at both ends and stretched to a displacement of 8.43 mm at a loading rate of 0.125 mm/min, followed by a 3600 s hold for stress relaxation. The specimen was unloaded at a rate of 15 N/min, and the recovery displacement was measured for 30 minutes. To ensure stable data acquisition, a preload of 10^{-4} N was applied throughout the recovery measurement.

As a result, Figs. 2(c) and (d) show the experimental results of the SMP at a low temperature of 35 °C. Up to approximately 4000 s, the strain increases linearly, and the nominal stress increases with plastic deformation. During stress relaxation, the stress decreases over time. After unloading, a permanent strain remains in the SMP.

The stress–strain curves at 65 °C and 35 °C are shown in Figs. 2(e) and (f), respectively; the simulation results will be discussed in Section 5.1. At high temperatures, SMP exhibits characteristics typical of viscoelastic materials, where stress increases in a hyperelastic manner, holding the strain induces stress relaxation, and unloading facilitates recovery to the original configuration. At low temperatures, SMP behaves as a viscoplastic material, where plastic deformation and stress relaxation occur, and unloading results in permanent strain.

4.4. Volume fraction test

A stress relaxation test was conducted to estimate the volume fraction. The specimen geometry is shown in Fig. A.2, with a thickness of 1 mm. Initially, the specimen was stretched to approximately 80% of its original length at a rate of 0.125 mm/min, while maintaining a constant temperature of 35 °C. The specimen was then held for stress relaxation for 3600 s. Next, the temperature was increased from $T_l = 35$ °C to $T_h = 65$ °C at a rate of 1 °C/min, while maintaining the strain, and the stress evolution was measured. After the temperature reached 65 °C, unloading was performed to terminate the experiment. The stress evolution data was substituted into Eq. (3) to calculate the

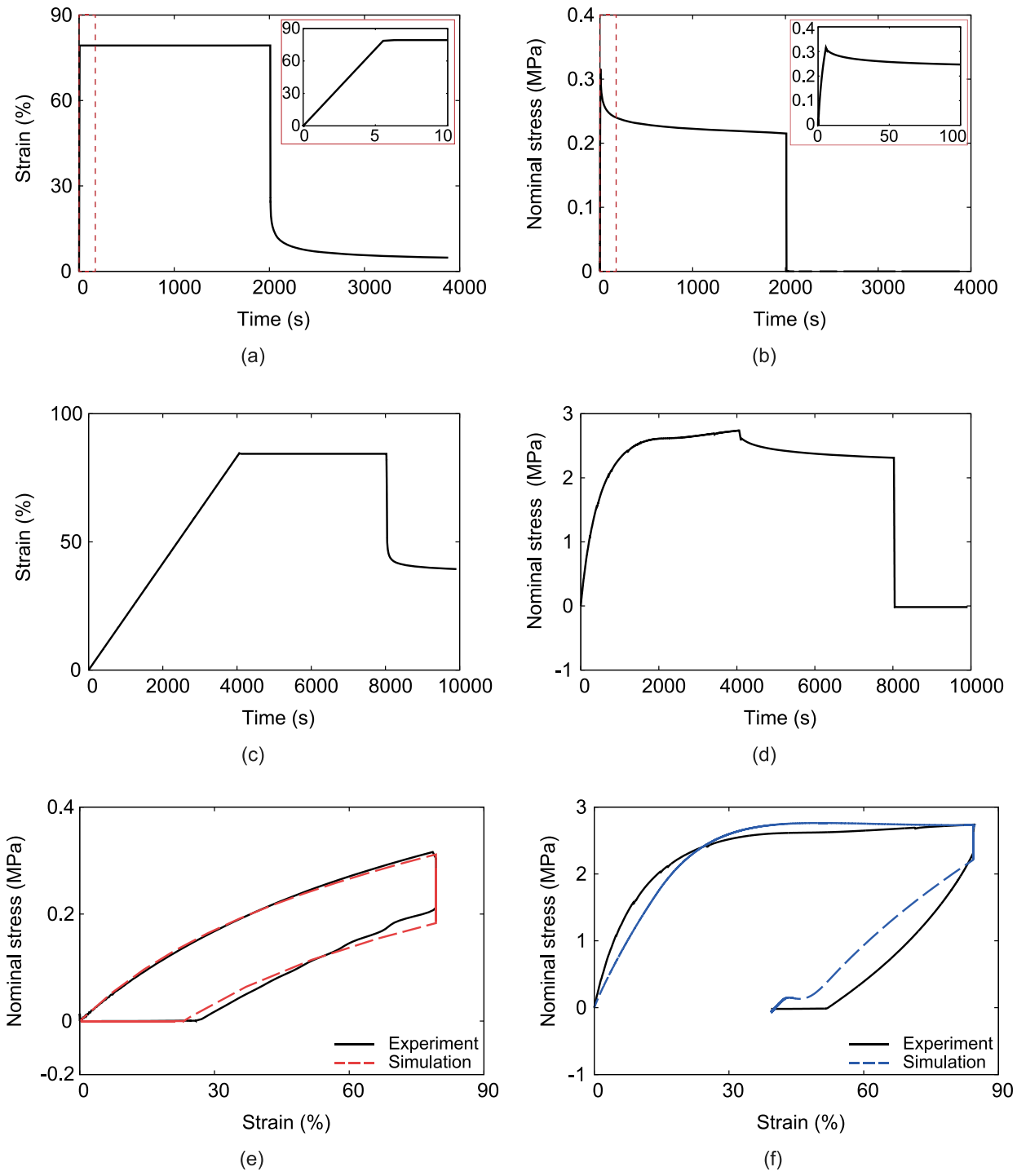

Fig. 2. Experimental results of SMP: (a) Strain versus time and (b) nominal stress versus time at 65 °C; the insets in (a) and (b) show the response from 0 to 10 s and 0 to 100 s, respectively, for clarity. (c) Strain versus time and (d) nominal stress versus time at 35 °C. (e, f) Nominal stress versus strain at 65 °C and 35 °C, respectively. The simulation results will be discussed in Section 5.1.

glassy volume fraction, and the regression of the glassy volume fraction was performed using Eq. (4).

As a result, Fig. 3(a) shows the graph of stress versus temperature during stress evolution. With strain held constant, the stress decreases as the temperature increases. Fig. 3(b) presents the graphs of glassy volume fraction versus temperature, obtained from both the experiment and regression. The corresponding coefficients from the regression are summarized in Table 1. The rubbery volume fraction can be calculated as $\xi_r = 1 - \xi_g$.

4.5. Uniaxial thermo-mechanical testing across a wide temperature range

A uniaxial thermo-mechanical test was performed over a wide temperature range to expose the SMPs to three distinct phases. For the DMA analysis, the SMP specimen was fabricated with dimensions of $30 \times 6 \times 1.5$ mm^3. The specimen was initially stretched to approximately 80% of its original length at a constant temperature of $T_h = 65$ °C, with a displacement rate of 11.984 mm/min. The specimen was then cooled to room temperature (20 °C) while maintaining the displacement. After

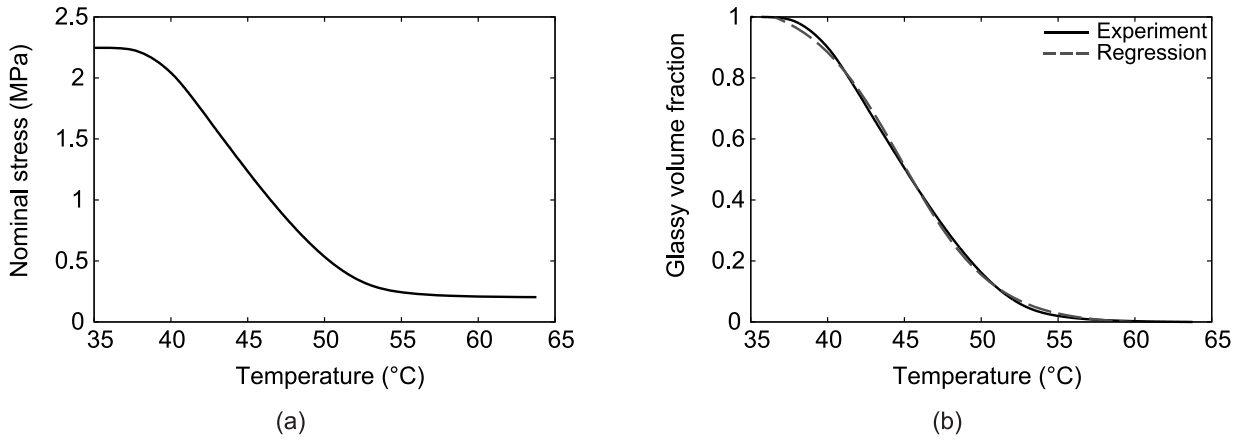

Fig. 3. Volume fraction test: (a) Response of SMP under thermo-mechanical conditions, and (b) glassy volume fraction obtained from both experiment and regression.

Table 1
Coefficients for the glassy volume fraction formulation in Eq. (4).

a	b $(°C^{-1})$	T_{tr}	d
1.0710	0.3326	44.8155	0.0073

Table 2
Optimized coefficients for the three-phase model: rubbery, glassy, and crystalline phases.

Rubbery	$C^e_{10,r}$ 0.067 MPa	$C^e_{01,r}$ 0.0695 MPa	$C^v_{10,r}$ 0.128 MPa	$C^v_{01,r}$ 0.127 MPa	μ_r 0.101 GPa·s
Glassy	$C^e_{10,g}$ 1.5 MPa	$C^e_{01,g}$ 1.5 MPa	$C^v_{10,g}$ 6.5 MPa	$C^v_{01,r}$ 6.5 MPa	μ_g 0.7 GPa·s
	σ^Y 2 MPa	E^p 18 MPa	μ^p_g 16 GPa·s		
	α 0.49 /s	β 0.929			
Crystalline	T_c 22°C	k_c 2×10^{-3}/s	γ 1	ζ −0.22 MPa/°C	

cooling, the force was measured for 30 min while holding the displacement. Next, unloading was carried out at a release rate of 15 N/min, with the temperature maintained at 20 °C, and the displacement was measured. After unloading, the recovery displacement was measured for 300 s at 20 °C. Finally, the temperature was increased to 65 °C at a rate of 20 °C/min, and the displacement change was measured.

As shown in Fig. 4, the response of SMP during the thermo-mechanical test is presented; the simulation plot will be discussed in Section 5.2. During the initial stress relaxation process up to 547 s, the stress decreased to 0.1776 MPa. Subsequently, crystallization occurred as the temperature remained below the crystallization threshold, and the stress increased to 0.3907 MPa. The unloading process reduced the stress to zero, while a permanent strain was formed. Following the recovery process, the increase in temperature caused the SMP to return to its original configuration.

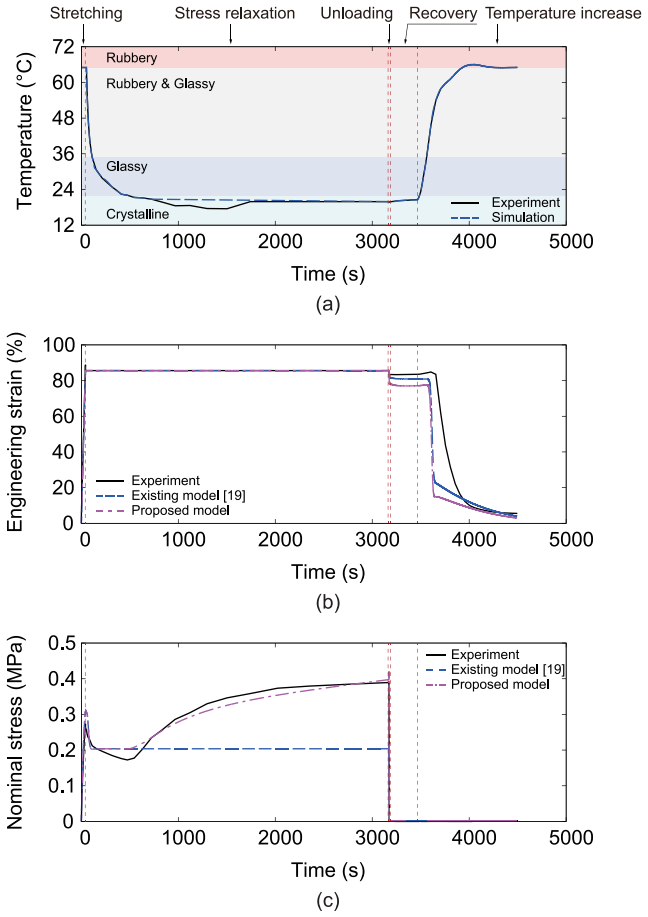

Fig. 4. Comparison of thermo-mechanical tests on SMP between experiment and simulation: (a) Time-dependent temperature conditions, (b) strain versus time, and (c) stress versus time.

5. Numerical analyses

5.1. Numerical model for the isothermal phase

Rubbery and glassy phase models are developed to describe the behavior of SMP at constant temperatures of 65 °C and 35 °C, respectively, consistent with the experiments described in Section 4.3. The rubbery phase model consists of hyperelastic and viscoelastic components. The corresponding constitutive equations are provided in Eqs. (8)–(10) and involve four coefficients: $C^e_{10,r}$, $C^e_{01,r}$, $C^v_{10,r}$, and $C^v_{01,r}$, related to hyperelasticity, and one viscosity coefficient μ_r. The glassy phase numerical model comprises a hyperelastic component with coefficients $C^e_{10,g}$ and $C^e_{01,g}$, a viscoelastic component with coefficients $C^v_{10,g}$, $C^v_{01,g}$, and μ_g, a viscoplastic component with coefficients σ^Y, E^p, and μ^p_g, and a shape memory strain component with coefficients α and β. The shape memory strain component is not activated in the fully glassy phase. We apply the same thermo-mechanical boundary conditions as those used in the experimental tests in Section 4.3. The rubbery and glassy coefficients activated in the isothermal simulation are optimized and summarized

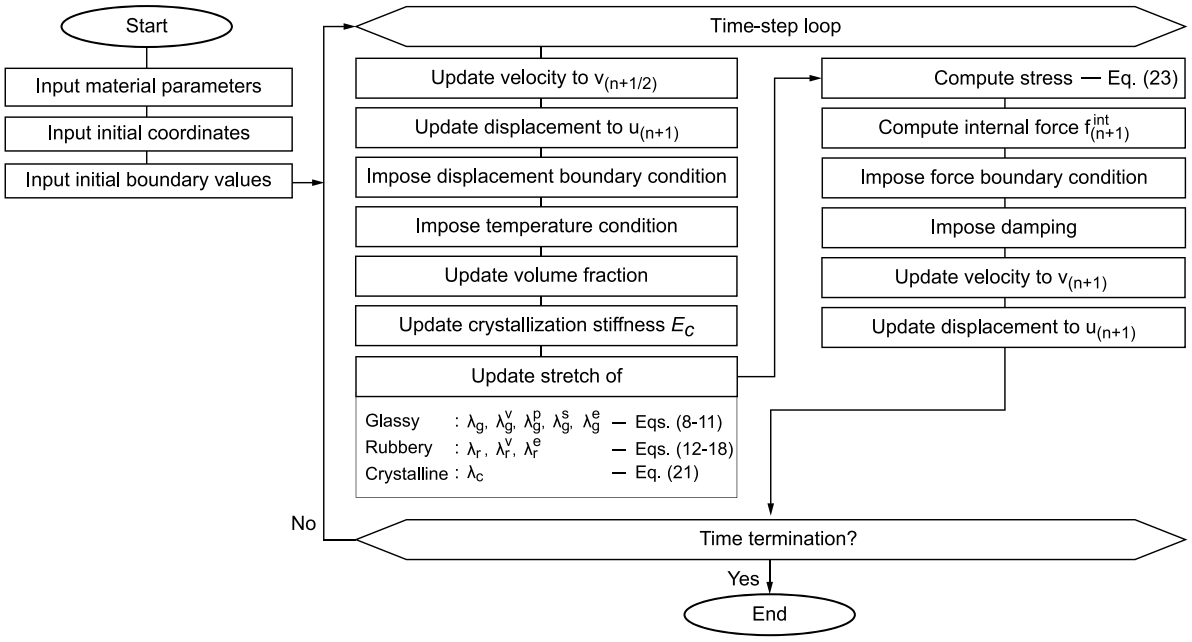

Fig. A.1. Flowchart of the algorithm for the three-phase model using Velocity-Verlet integration.

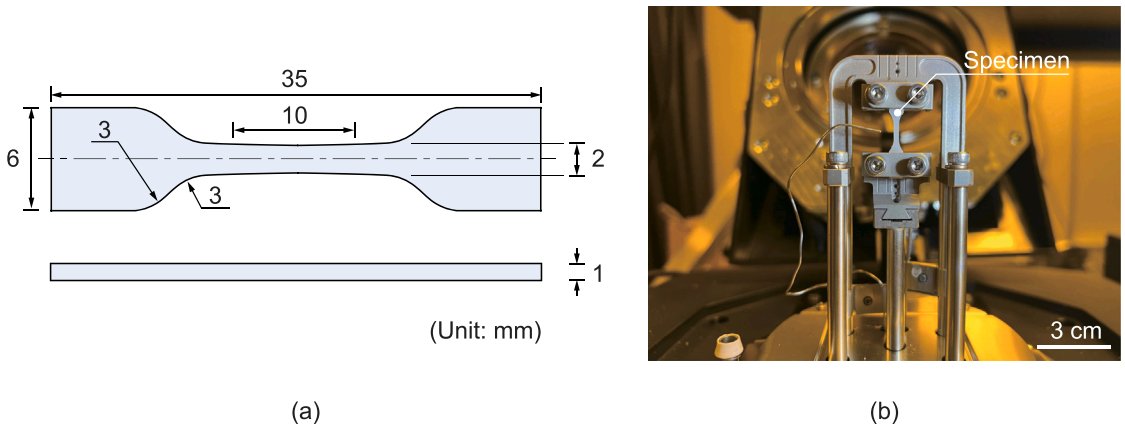

Fig. A.2. Experiment setup: (a) Dumbbell-shaped ISO 37 Type 4 geometry of the shape memory polymer (SMP) specimen with a thickness of 1 mm and (b) the specimen gripped in the dynamical mechanical analysis (DMA) machine.

in rows 1 through 6 of Table 2. The flowchart in Fig. A.1 is implemented using MATLAB to simulate the proposed three-phase model.

As a result, Figs. 2(e) and (f) show the graphs of stress versus strain for the rubbery and glassy phases, respectively, in comparison with the experimental results. The simulation results are in good agreement with the experimental data.

5.2. Numerical thermo-mechanical test

The thermo-mechanical test in Section 4.5 is numerically analyzed using the proposed three-phase model, which includes the rubbery, glassy, and crystalline phases, as shown in Fig. 1. The corresponding constitutive equations are written in Eqs. (8) to (23). As the temperature varies during the test, both the shape memory strain and thermal elasticity might increase. The coefficients for shape memory strain (α and β) and the coefficients for the crystallization phase (k_c, γ, and ζ) are set to the values summarized in rows 7 through 10 of Table 2. The experimental temperature conditions are filtered and applied to simulations, as shown in Fig. 4(a). In this figure, each phase is highlighted according to the corresponding temperature range.

As shown in Figs. 4(b) and (c), the SMP responses from the experiment, existing model, and proposed model are presented. As the specimen is stretched, both strain and nominal stress increase. During stress relaxation, as the temperature decreases and is maintained at a low level to keep the SMP in the crystalline phase, the stress initially relaxes and then increases after 547 s as the SMP transitions into the crystalline phase. During unloading at low temperatures, the stress decreases to zero while the strain is maintained. As temperature increases, the deformed SMP almost recovers its original configuration; interestingly, the strain does not fully return to zero, which is consistent with the experimental data. As shown in Fig. 4(b), the original model, which excludes the crystalline phase, results in constant stress during stress relaxation at 20 °C. In contrast, the proposed model captures the increase in stress during stress relaxation at low temperatures, which aligns with the experimental data.

6. Conclusion

This study investigates the behavior of thermally activated shape memory polymers (SMPs) across a wide temperature range, including the rubbery, glassy, and crystalline regions, and proposes a three-phase

Table A.3
Summary of model parameters and their corresponding optimization procedures.

Phase	Component	Parameter	Physical meaning	Optimization order within phase	Data for RMSE	RMSE calculation range
Rubbery	Hyperelastic	$C^e_{10,r}$	Mooney–Rivlin coefficient	1	Stress vs. strain at T_h	Loading part
		$C^e_{01,r}$	Mooney–Rivlin coefficient	2	Stress vs. strain at T_h	Loading part
	Viscoelastic	$C^v_{10,r}$	Mooney–Rivlin coefficient	3	Stress vs. strain at T_h	Unloading part
		$C^v_{01,r}$	Mooney–Rivlin coefficient	4	Stress vs. strain at T_h	Unloading part
		μ_r	Viscosity	5	Stress vs. strain at T_h	Unloading part
Glassy	Hyperelastic	$C^e_{10,g}$	Mooney–Rivlin coefficient	1	Stress vs. strain at T_l	Loading and unloading part
		$C^e_{01,g}$	Mooney–Rivlin coefficient	2	Stress vs. strain at T_l	Loading and unloading part
	Viscoelastic	$C^v_{10,g}$	Mooney–Rivlin coefficient	3	Stress vs. strain at T_l	Loading and unloading part
		$C^v_{01,g}$	Mooney–Rivlin coefficient	4	Stress vs. strain at T_l	Loading and unloading part
		μ_g	Viscosity	8	Stress vs. strain at T_l	Loading and unloading part
	Viscoplastic	σ^Y	Yield strength	5	Stress vs. strain at T_l	Loading and unloading part
		μ^p_g	Viscosity	6	Stress vs. strain at T_l	Loading and unloading part
		E^p	Hardening modulus	7	Stress vs. strain at T_l	Loading and unloading part
	Shape memory strain	α	Formation rate of shape memory strain	10	Force vs. time (thermo-mechanical test)	From 0 to 1000 s
		β	Max fraction of total strain	9	Force vs. time (thermo-mechanical test)	From 0 to 1000 s
Crystalline	Thermal elasticity	T_c	Crystallization temperature	Set by DSC	Force vs. time (thermo-mechanical test)	From 0 to 3177 s
		γ	Maximum saturation ratio	Default	Force vs. time (thermo-mechanical test)	From 0 to 3177 s
		ζ	Slope of modulus increase	1	Force vs. time (thermo-mechanical test)	From 0 to 3177 s
		k_c	Crystallization growth rate	2	Force vs. time (thermo-mechanical test)	From 0 to 3177 s

phenomenological model. SMP samples are fabricated using polycyclooctene (PCO) and dibenzoyl peroxide (DBzP). Isothermal tests are conducted at both high and low temperatures to examine the behavior of SMPs in the rubbery and glassy phases, respectively. At high temperatures, SMP exhibits characteristics typical of viscoelastic materials, where loading increases stress in a hyperelastic manner, holding the strain induces stress relaxation, and unloading restores the material to its original configuration. At low temperatures, the SMP behaves like a viscoplastic material, where loading increases the stress, plastic strain and stress relaxation occur, and unloading results in permanent strain. Additionally, thermo-mechanical tests are conducted to assess the SMP response across a broad temperature range. It is observed that a temperature drop in the stretched state leads to permanent strain once the load is removed. Upon subsequent temperature increases, the SMP nearly recovers its original configuration. These isothermal and thermo-mechanical tests are used to develop a numerical model for SMPs. For numerical analysis, models of the rubbery and glassy phases are developed to describe the results of the isothermal tests. The shape memory strain component in the glassy phase and the thermal elasticity in the crystalline phase are optimized based on the thermo-mechanical test. As a result, the proposed three-phase model demonstrates the potential to predict SMP behavior across a wide temperature range. While the developed numerical model is based on experimental data, further validation under a wide range of thermo-mechanical conditions is essential. Future work will focus on applying the model to additional experimental conditions to provide a more comprehensive validation and enhance the predictive capabilities of models under varying temperatures, strains, and loading scenarios. While the experiments are performed at a fixed cooling rate, the numerical model is formulated to accommodate variable thermal histories. Future studies incorporating experimental data under different cooling rates would provide further evaluation of the predictability of the model for crystallization kinetics. The current model is formulated within a one-dimensional uniaxial framework using scalar measures of deformation. Since frame rotation does not occur in this configuration, the use of an objective stress rate is not required (Simo and Hughes, 1998). However, for future extension to general three-dimensional loading conditions, the incorporation of objective stress rates, such as the upper-convected derivative, would be essential to ensure frame invariance.

CRediT authorship contribution statement

Suyeong Jin: Writing – original draft, Methodology, Funding acquisition, Formal analysis, Conceptualization. **Gunho Kim:** Writing – original draft, Methodology, Formal analysis, Conceptualization. **Seola Lee:** Methodology, Formal analysis. **Kamakshi Subramanian:** Methodology, Formal analysis. **Jung-Wuk Hong:** Writing – review & editing, Supervision. **Chiara Daraio:** Writing – review & editing, Supervision, Funding acquisition.

Declaration of competing interest

The authors declare that they have no known competing financial interests or personal relationships that could have appeared to influence the work reported in this paper.

Acknowledgments

This work was supported by Basic Science Research Program through the National Research Foundation of Korea (NRF) funded by the Ministry of Education, Korea (No. RS-2023-00242455); CD and GK

acknowledge support from Caltech's Merkin Institute for Translational Research (No. 13520291), Rothenberg Innovation Initiative (RI 2) (No. 25570017 and 25570029), and the Heritage Medical Research Institute (HMRI), United States (No. HMRI-15-09-01). We gratefully acknowledge Max Kudisch for providing helpful feedback during the preparation of this work.

Appendix. Supplementary information

A.1. Flowchart of the SMP

The three-phase model is implemented using the Velocity-Verlet algorithm (Ercolessi, 1997). Fig. A.1 shows the flowchart of the implemented code. Material parameters, initial coordinates, time-varying boundary conditions are input, and the response of the SMP is simulated in the time-step loop. During the loop, the behaviors of the rubbery, glassy, and crystalline phases are calculated and superposed to determine the stress in the SMP.

A.2. Experiment setup

See Fig. A.2.

A.3. Parameter optimization procedure

A total of 19 parameters listed in Table 2 are optimized using a root mean square error (RMSE) criterion, defined as

$$\mathrm{RMSE} = \sqrt{\frac{1}{n}\sum_{i=1}^{n}\left(\hat{y}\left(x_i\right) - y\left(x_i\right)\right)^2}, \tag{A.1}$$

where $\hat{y}\left(x_i\right)$ and $y\left(x_i\right)$ represent the simulated and experimental results, respectively, measured at an internal variable x_i, and n is the number of measurements. The RMSE is calculated over different ranges of x_i for each parameter, reflecting the influence on the corresponding phase response. Each parameter is assigned the value that minimizes the RMSE. For example, in the case of the rubbery phase, we use the experimental data of nominal stress versus engineering strain obtained from isothermal uniaxial tests at high temperature, as described in Section 4.3. Five parameters related to the rubbery phase are optimized in the following order: $C^e_{10,r}, C^e_{01,r}, C^v_{10,r}, C^v_{01,r}, \mu_r$. The parameters $C^e_{10,r}$ and $C^e_{01,r}$ are optimized using the loading curve, while $C^v_{10,r}, C^v_{01,r}$, and μ_r are optimized based on the unloading curve. A summary of the optimization process and the corresponding range of the RMSE calculation for each parameter is presented in Table A.3.

Data availability

Data will be made available on request.

References

Al Azzawi, W., Herath, M., Epaarachchi, J., 2019. 15 - modeling, analysis, and testing of viscoelastic properties of shape memory polymer composites and a brief review of their space engineering applications. In: Guedes, R.M. (Ed.), Creep and Fatigue in Polymer Matrix Composites (Second Edition), second ed. In: Woodhead Publishing Series in Composites Science and Engineering, Woodhead Publishing, pp. 465–495. http://dx.doi.org/10.1016/B978-0-08-102601-4.00015-1.

Boyle, A.J., Landsman, T.L., Wierzbicki, M.A., Nash, L.D., Hwang, W., Miller, M.W., Tuzun, E., Hasan, S.M., Maitland, D.J., 2016. In vitro and in vivo evaluation of a shape memory polymer foam-over-wire embolization device delivered in saccular aneurysm models. J. Biomed. Mater. Res. Part B: Appl. Biomater. 104 (7), 1407–1415. http://dx.doi.org/10.1002/jbm.b.33489.

Callister Jr., W.D., Rethwisch, D.G., 2020. Materials Science and Engineering: an Introduction. John wiley & sons.

Chen, Y.-C., Lagoudas, D.C., 2008. A constitutive theory for shape memory polymers. Part I: Large deformations. J. Mech. Phys. Solids 56 (5), 1752–1765. http://dx.doi.org/10.1016/j.jmps.2007.12.005.

Ercolessi, F., 1997. A molecular dynamics primer. Spring College in Computational Physics, ICTP,

Ge, Q., Sakhaei, A.H., Lee, H., Dunn, C.K., Fang, N.X., Dunn, M.L., 2016. Multimaterial 4D printing with tailorable shape memory polymers. Sci. Rep. 6 (1), 31110. http://dx.doi.org/10.1038/srep31110.

Holzapfel, G.A., 2002. Nonlinear solid mechanics: A continuum approach for engineering science. Meccanica 37 (4), 489–490. http://dx.doi.org/10.1023/A:1020843529530.

Kim, J.H., Kang, T.J., Yu, W.-R., 2010. Thermo-mechanical constitutive modeling of shape memory polyurethanes using a phenomenological approach. Int. J. Plast. 26 (2), 204–218. http://dx.doi.org/10.1016/j.ijplas.2009.06.006.

Lendlein, A., Langer, R., 2002. Biodegradable, elastic shape-memory polymers for potential biomedical applications. Science 296 (5573), 1673–1676. http://dx.doi.org/10.1126/science.1066102.

Leng, J., Lan, X., Liu, Y., Du, S., 2011. Shape-memory polymers and their composites: Stimulus methods and applications. Prog. Mater. Sci. 56 (7), 1077–1135. http://dx.doi.org/10.1016/j.pmatsci.2011.03.001.

Liu, C., Chun, S.B., Mather, P.T., Zheng, L., Haley, E.H., Coughlin, E.B., 2002. Chemically cross-linked polycyclooctene: Synthesis, characterization, and shape memory behavior. Macromolecules 35 (27), 9868–9874. http://dx.doi.org/10.1021/ma021141j.

Liu, Y., Gall, K., Dunn, M.L., Greenberg, A.R., Diani, J., 2006. Thermomechanics of shape memory polymers: Uniaxial experiments and constitutive modeling. Int. J. Plast. 22 (2), 279–313. http://dx.doi.org/10.1016/j.ijplas.2005.03.004.

Mailen, R.W., Liu, Y., Dickey, M.D., Zikry, M., Genzer, J., 2015. Modelling of shape memory polymer sheets that self-fold in response to localized heating. Soft Matter 11, 7827–7834. http://dx.doi.org/10.1039/C5SM01681A.

Park, H., Harrison, P., Guo, Z., Lee, M.-G., Yu, W.-R., 2016. Three-dimensional constitutive model for shape memory polymers using multiplicative decomposition of the deformation gradient and shape memory strains. Mech. Mater. 93, 43–62. http://dx.doi.org/10.1016/j.mechmat.2015.10.014.

Posada-Murcia, A., Uribe-Gomez, J.M., Förster, S., Sommer, J.-U., Dulle, M., Ionov, L., 2022. Mechanism of behavior of two-way shape memory polymer under constant strain conditions. Macromolecules 55 (5), 1680–1689.

Qi, H.J., Nguyen, T.D., Castro, F., Yakacki, C.M., Shandas, R., 2008. Finite deformation thermo-mechanical behavior of thermally induced shape memory polymers. J. Mech. Phys. Solids 56 (5), 1730–1751. http://dx.doi.org/10.1016/j.jmps.2007.12.002.

Risso, G., Kudisch, M., Ermanni, P., Daraio, C., 2024. Tuning the properties of multistable structures post-fabrication via the two-way shape memory polymer effect. Adv. Sci. 11 (21), 2308903. http://dx.doi.org/10.1002/advs.202308903.

Shojaei, A., Xu, W., Yan, C., Yang, Q., Li, G., 2022. Insight in thermomechanical constitutive modeling of shape memory polymers. Front. Mech. Eng. 8, http://dx.doi.org/10.3389/fmech.2022.956129.

Simo, J., Hughes, T., 1998. In: Marsden, J., Sirovich, L., Wiggins, S. (Eds.), Computational Inelasticity, vol. 7, Springer-Verlag New York.

Tobushi, H., Hashimoto, T., Hayashi, S., Yamada, E., 1997. Thermomechanical constitutive modeling in shape memory polymer of polyurethane series. J. Intell. Mater. Syst. Struct. 8 (8), 711–718. http://dx.doi.org/10.1177/1045389X9700800808.

Tobushi, H., Okumura, K., Hayashi, S., Ito, N., 2001. Thermomechanical constitutive model of shape memory polymer. Mech. Mater. 33 (10), 545–554. http://dx.doi.org/10.1016/S0167-6636(01)00075-8.

Wang, K., Jia, Y.-G., Zhao, C., Zhu, X., 2019. Multiple and two-way reversible shape memory polymers: Design strategies and applications. Prog. Mater. Sci. 105, 100572. http://dx.doi.org/10.1016/j.pmatsci.2019.100572.

Wei, H., Liu, L., Zhang, Z., Du, H., Liu, Y., Leng, J., 2015. Design and analysis of smart release devices based on shape memory polymer composites. Compos. Struct. 133, 642–651. http://dx.doi.org/10.1016/j.compstruct.2015.07.107.

Xia, Y., He, Y., Zhang, F., Liu, Y., Leng, J., 2021. A review of shape memory polymers and composites: Mechanisms, materials, and applications. Adv. Mater. 33 (6), 2000713. http://dx.doi.org/10.1002/adma.202000713.

Xiao, X., Kong, D., Qiu, X., Zhang, W., Zhang, F., Liu, L., Liu, Y., Zhang, S., Hu, Y., Leng, J., 2015. Shape-memory polymers with adjustable high glass transition temperatures. Macromolecules 48 (11), 3582–3589. http://dx.doi.org/10.1021/acs.macromol.5b00654.

Yan, C., Li, G., 2022. Tutorial: Thermomechanical constitutive modeling of shape memory polymers. J. Appl. Phys. 131 (11), 111101. http://dx.doi.org/10.1063/5.0080897.

Zeng, H., Sun, H., Gu, J., 2021. Modeling the one-way and two-way shape memory effects of semi-crystalline polymers. Smart Mater. Struct. 30 (9), 095020. http://dx.doi.org/10.1088/1361-665X/ac179e.